Heterostructural amorphous catalysts decorated membranes with excellent anti-fouling performances in wastewater purification

Yuling Yang [a, c], Yingxin Zhang [b], Ping Zhu [a], Gang Wang [a], Zhanghui Wang [d], Lijing Zhu [a, *], Zhixiang Zeng [a, *]

[a] *State Key Laboratory of Advanced Marine Materials, Ningbo Institute of Materials Technology and Engineering, Chinese Academy of Sciences, Ningbo 315201, China*

[b] *School of Materials & Chemical Engineering, Ningbo University of Technology, Ningbo 315211, China*

[c] *Center of Materials Science and Optoelectronics Engineering, University of Chinese Academy of Sciences, Beijing 100049, China*

[d] *School of Materials Science and Engineering, NingboTech University, Ningbo 315100, China*

***Corresponding Authors:**

Dr. Lijing Zhu

E-mail: zhulijing@nimte.ac.cn

Prof. Zhixiang Zeng

E-mail: zengzhx@nimte.ac.cn

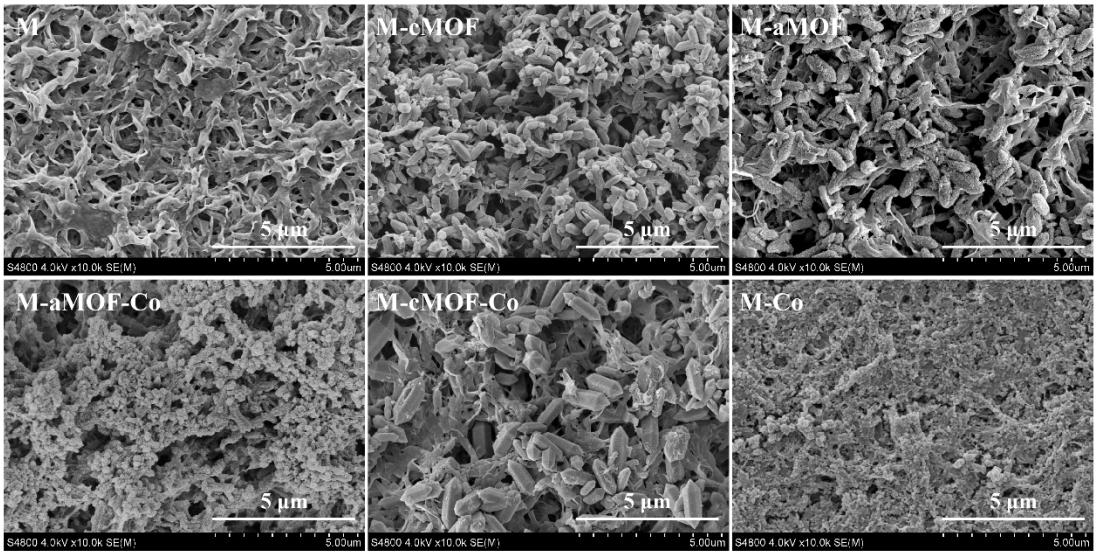

Fig. S1. SEM images of M, M-cMOF, M-aMOF, M-aMOF-Co, M-cMOF-Co, and M-Co.

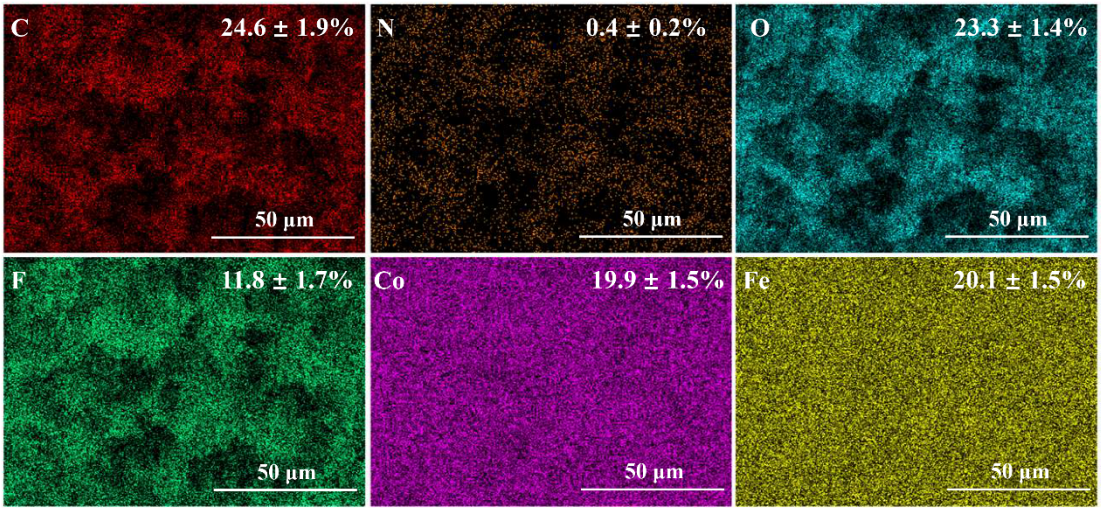

Fig. S2. The surface SEM-EDS mapping and element contents of M-aMOF-Co.

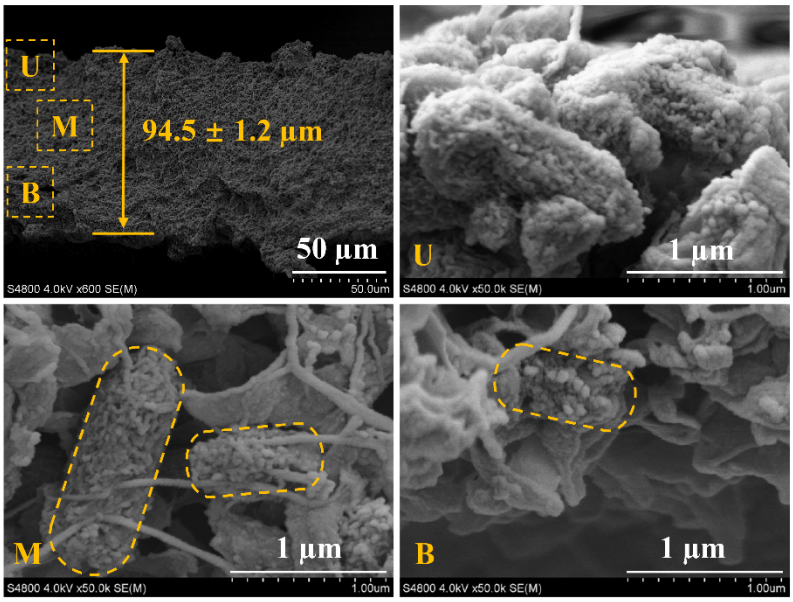

Fig. S3. The cross-sectional SEM images of M-aMOF-Co.

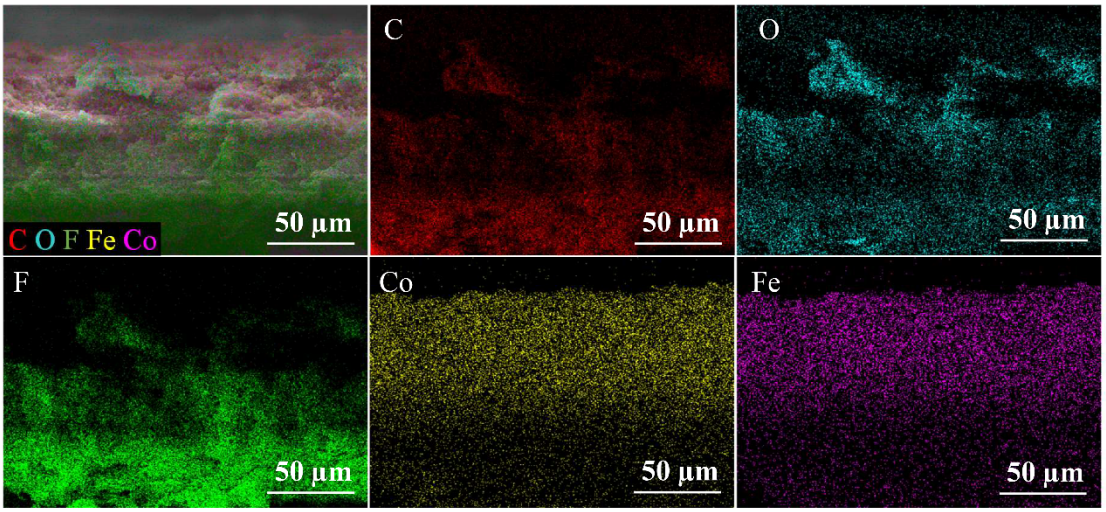

Fig. S4. The SEM-EDS mapping images on the cross-sectional of M-aMOF-Co.

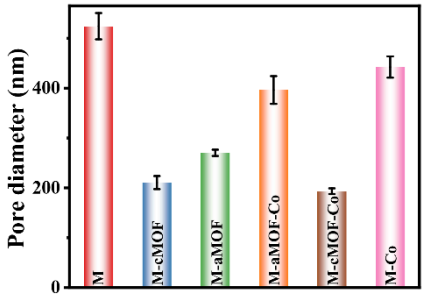

Fig. S5. Pore size of the membranes.

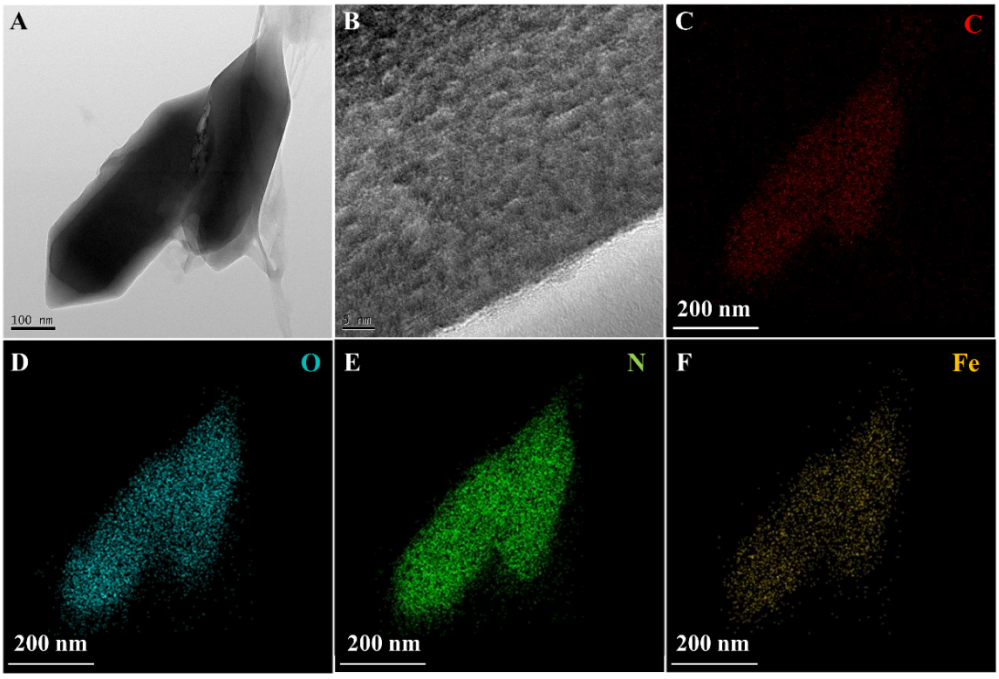

Fig. S6. (A, B) HR-TEM images and (C-F) EDS mapping images of cMOF after being scraped from M-cMOF.

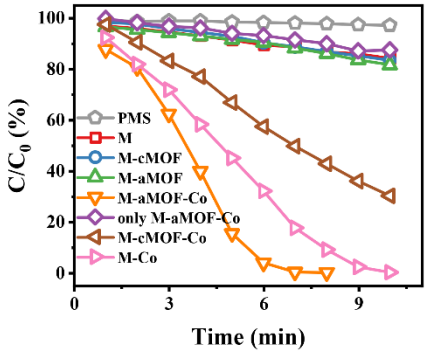

Fig. S7. Temporal evolution of MB concentration in the presence of diverse membranes and PMS solutions.

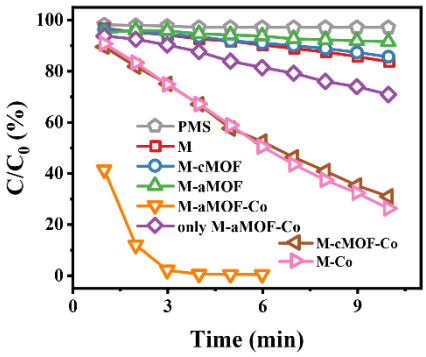

Fig. S8. Temporal evolution of Rh B concentration in the presence of diverse membranes and PMS solutions.

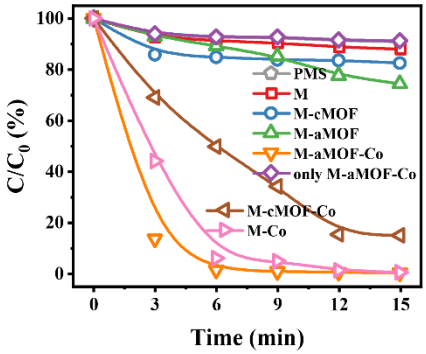

Fig. S9. Temporal evolution of LEVO concentration in the presence of diverse membranes and PMS solutions.

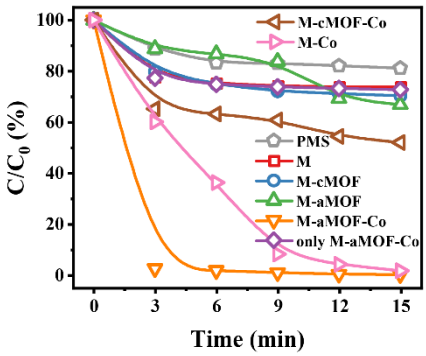

Fig. S10. Temporal evolution of ENR concentration in the presence of diverse membranes and PMS solutions.

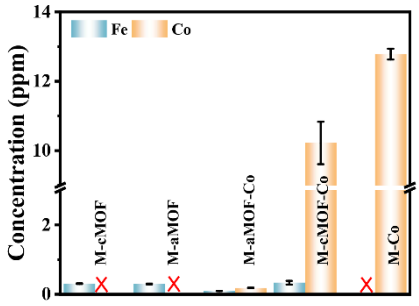

Fig. S11. Fe and Co contents in the washing solutions. They were used to wash the membranes for one week.

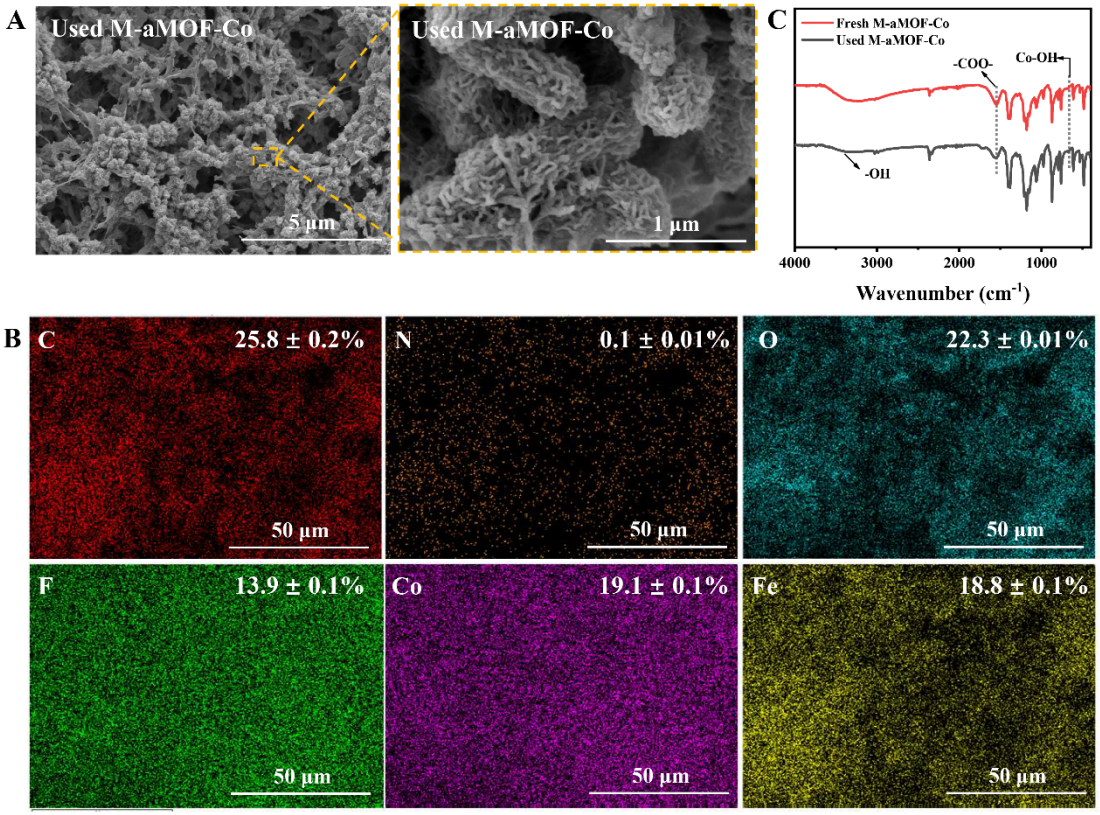

Fig. S12. (A) Surface SEM images, (B) EDS mapping images, and (C) FTIR of M-aMOF-Co after six consecutive TC degradation cycles followed by being immersed in water for 60 days.

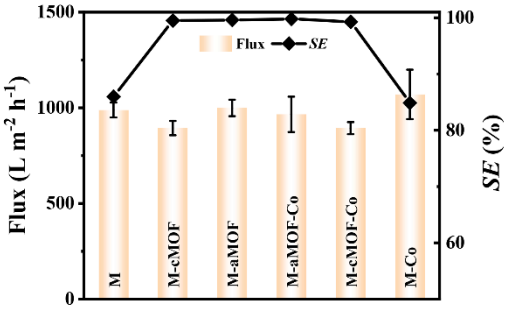

Fig. S13. Separation performance of the diverse membranes for tween 80-stabilized toluene-in-water emulsions.

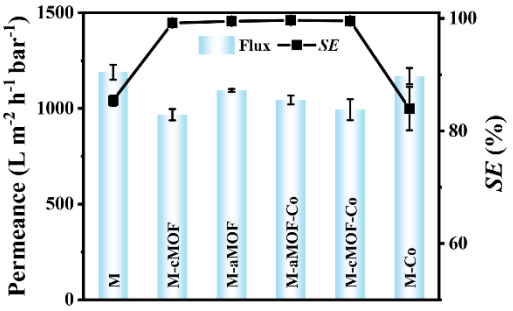

Fig. S14. Separation performance of the diverse membranes for tween 80-stabilized dichloromethane-in-water emulsion.

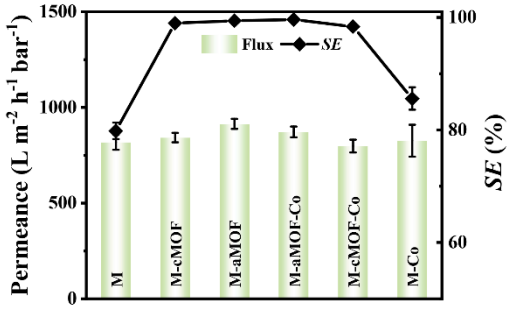

Fig. S15. Separation performance of the diverse membranes for tween 80-stabilized soybean oil-in-water emulsion.

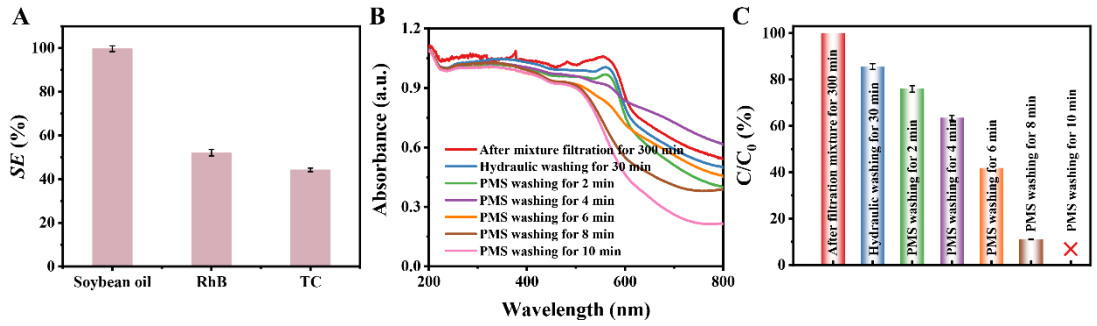

Fig. S16. (A) Separation efficiency of soybean oil-in-water emulsion, RhB, and TC of M-aMOF-Co. (B) UV-vis absorption spectroscopy of the used M-aMOF-Co after PMS washing for various times. (C) RhB content on M-aMOF-Co after being washed with PMS.

Table S1. XPS results of PVDF and the membranes.

Sample	C (%)	O (%)	N (%)	F (%)	Fe (%)	Co (%)
M	51.1 ± 0.1	1.34 ± 0.2	0	47.5 ± 0.3	0	0
M-cMOF	58.5 ± 0.3	17.9 ± 0.02	3.8 ± 0.1	18.4 ± 0.3	1.5 ± 0.01	0
M-aMOF	52.9 ± 0.2	16.5 ± 0.2	1.6 ± 0.1	25.9 ± 0.3	1.8 ± 0.01	1.3 ± 0.04
M-aMOF-Co	52.9 ± 0.3	23.7 ± 0.2	1.4 ± 0.1	15.9 ± 0.1	2.3 ± 0.1	3.7 ± 0.2
M-cMOF-Co	59.8 ± 0.4	18.3 ± 0.3	3.3 ± 0.1	17.2 ± 0.1	1.3 ± 0.3	0.1 ± 0.01
M-Co	50.4 ± 0.5	17.2 ± 0.1	0	27.2 ± 0.4	0	5.1 ± 0.3